

Transformation Mechanism of Dual-mode Penetrators Achieved by Single-point Detonation

Wei-bing Li*, Huan Zhou, Wen-bin Li, Xiao-ming Wang, and Jian-jun Zhu

School of Mechanical Engineering, Nanjing University of Science & Technology, Nanjing 210 094, China

**E-mail:njustlwb@163.com*

ABSTRACT

A shaped charge was produced with a wave shaper that can transform dual-mode penetrators by changing the single-point detonation location. Specifically, the theory of denotation wave formation was applied to analyse changes in the shaped charge liner surface pressure in different initiation situations. An analytical model was established of the projectile explosively formed by denotation at the top of the shaped charge liner and jetting projectile charge formed by denotation at the center of charge. LS-DYNA finite element simulation software was used to study the effects of the shaped charge liner configuration parameters on the formation of dual-mode penetrators, and orthogonal optimising design and simulation calculation was conducted to obtain suitable structural parameters of a uniform-thickness eccentric hemisphere shaped charge liner. X-ray imaging and penetration experiments were then conducted. The penetration depth of the explosively formed projectile in a steel target was $0.64 D_k$ the charge diameter, while that of the jetting projectile charge was $2.42 D_k$ when the burst height was approximately $13 D_k$.

Keywords: Single-point initiation; Explosively formed projectile; Jetting projectile charge; Explosive pressure; Numerical simulation

NOMENCLATURE

D_k	Charge diameter	R_1	Outer radius
$M(x)$	Liner element	ΔV	Head-tail velocity difference
$Pb(x)$	Pressure on the liner element when an explosive is detonating	V_j	Higher head velocity
$A_o(x)$	Cross-sectional area	ψ_r	Angle between detonation wave front and charge symmetry axis
$V(x)$	Speed	ψ_0	Incident angle
$dM(x)$	Liner element weight	α	Turning inward
ρ	Density	γ	Exponent of the product of explosive gas
$h(x)$	Thickness	ψ_1	Intersection angle of reflected shock waves
$t_1(x)$	Time that denotation waves pass the corresponding liner element	δ	Turning angle
D	Detonation velocity	λ	Incoming flow
$dm(x)$	Weight of an explosive element		
$l(x)$	Length of an explosive element		
L	Charge length		
$f[l(x)/L]$	Correction term		
R_i	Distance between the initiation point and the charge symmetry axis		
H_i	Distance between projected point of initiation point on charge symmetry axis and crossing point of the detonation wave front and charge symmetry axis		
M_2	Mach number of area II		
P_H	Pressure of the C-J denotation wave front		
h	Thickness of liner		
H	Height of the top of liner		

1. INTRODUCTION

The multi-mode warhead is attracting attention from researchers around the world for its outstanding advantages of multiple mechanisms of destruction, great inflicted damage and high cost-effectiveness against a background of high-tech local wars breaking out more frequently, increasing complexity of battlefield targets, and the protection level of weapons continuously improving. Fong¹ and Lawther² proposed the installation of a grille and an alternative method of detonation for penetrator transformation. Later, Bender³ and Whelan⁴ used a multi-point detonation device to realise penetrator transformation, but at the same time, it also brings the effect of the synchronisation of the multi-point detonation device. Li⁵, *et al.* thus investigated the effect of an annular multi-point detonation device on the formation and penetration capacity of penetrators. They found the number of optimum

multi-point initiations which can successfully substitute for the traditional peripheral initiation under a certain charge calibre, and determined that the initiation deviation should be 200 ns to ensure the penetrator does not bend or transform. However, it is difficult to control the initiation deviation of a multi-point initiation device in practice. Graswald⁶ and Arnold⁷, *et al.* advanced the high-explosive pellet to realise the transformation of penetrators, which solved the problem of synchronisation associated with a multi-point initiation device. However, their approach is problematic in that it is difficult to process and control penetrators and thus achieve the best penetration capacity. Li⁷, *et al.* tested and verified the feasibility of the transformation of penetrators through a simple change in the single-point initiation position, but how to improve the maximum power of various penetrators using a single-point initiation device and the transformation mechanism of damage modes for different initiation points requires further research.

Using a shaped charge and a wave shaper, the present study transformed an explosively formed projectile (EFP) and jetting projectile charge (JPC) through a simple change in the single-point initiation position. The theory of denotation wave formation was applied to analyse the formation mechanism of penetrators at each initiation position, and LS-DYNA finite element simulation software was used to investigate the effect of the shaped charge liner configuration parameters on the formation of dual-mode penetrators. Orthogonal optimising design and simulation calculations were conducted to obtain good structural parameters of the shaped charge liner, and X-ray imaging and penetration experiments were performed to test and verify the design of dual-mode transformation.

2. MECHANISM OF DUAL-MODE PENETRATORS FORMATION

With regard to a shaped charge having a specific structure, the compression and deformation tendency of the liner surface depends on the distribution of the detonation load transmitted by different initiation mechanisms. Hence, the front structure of the denotation wave shaped by different initiation mechanisms decides the distribution of the detonation load and the formation of penetrators. This study used the shaped-charge configuration of a small length/radius ratio and a wave shaper to realise the transformation of an EFP and JPC that have better formability through a simple change in the single-point initiation position.

2.1 Formation Mechanism of the EFP

Figure 1 is a sketch of a charge with a wave shaper, showing the charge is a single-point initiation device when the initiation position is at the top of the shaped charge liner. According to relevant studies^{9,10}, under the condition of single-point initiation, the charge only produces C-J detonation waves rather than a Mach wave. As the denotation waves move outward away from the shaped charge liner, they put less pressure on the shaped charge liner, which can be simplified as one-dimensional projectile motion of the shaped charge liner element from the corresponding explosive element.

As shown in Fig. 1, the liner element $M(x,y)$ is moved to the right by the explosive element with spherical denotation waves spreading to the left. This study applies the loading

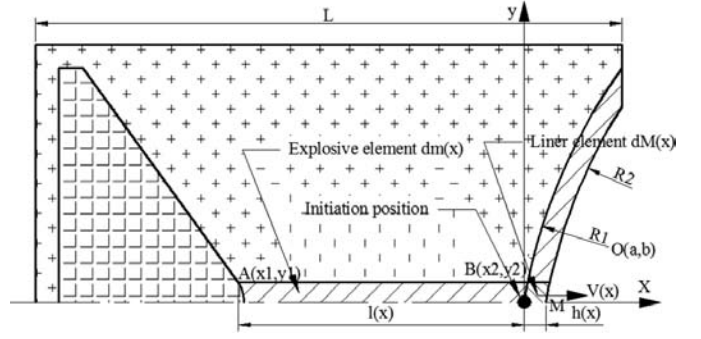


Figure 1. One dimensional motion of liner element when it formed at initiation top point of liner.

theory of the explosive's push on an object to analyse the effect of the detonation product on the liner¹¹. According to Newton's second law of motion,

$$P_b(x) \cdot A_0(x) = -dM(x) \frac{dv(x)}{dt_1(x)}, \quad (1)$$

$$dM(x) = A_0(x) \cdot h(x) \cdot \rho, \text{ and} \quad (2)$$

$$t_1(x) = t - \frac{\sqrt{x^2 + y^2}}{D}, \quad (3)$$

where $P_b(x)$ is the pressure on the liner element when an explosive is detonating; $A_0(x)$, $v(x)$, $dM(x)$, ρ , and $h(x)$ respectively represent the cross-sectional area, speed, liner element, weight, and density of the liner element; $t_1(x)$ is the time that denotation waves pass the corresponding liner element; and D is the detonation velocity of the explosive.

Through the integral transformation of Eqn. (1), and considering the effect of the charge and the position of the liner element, the pressure on the liner element $P_b(x)$ can be deduced as

$$\frac{P_b(x)}{P_H} = \frac{64}{27} \left(\frac{1}{\sqrt{4 + \frac{32dm(x)}{27dM(x)} \cdot \frac{D}{l(x)} t_1(x)}} + f \left[\frac{l(x)}{L} \right] \right)^3, \quad (4)$$

where P_H is the denotation pressure of C-J detonation waves, $dm(x)$ and $l(x)$ are respectively the weight and length of an explosive element, L is the charge length, and $f[l(x)/L]$ is a correction term.

According to the above analysis, the pressure on the liner surface changing with time can be solved approximately. Because no Mach collision is generated and the denotation waves move outward from the liner, the pressure on the liner surface is lower than the denotation pressure of C-J detonation waves. Consequently, the liner overturns and forms the EFP under a modest detonation load.

2.2 Formation Mechanism of the JPC

As shown in Fig. 1, for the charge configuration, when the initiation point is situated at the center of charge, owing to the charge with wave shaper, the upper part of the wave shaper of the divergent detonation wave can get around wave shaper and transforms into a converging detonation wave with the shape of a ring array and is transmitted to the underlying explosive area. The approximate propagation and reflection of

the detonation wave are presented in Fig. 2, as discussed by Yanguo¹², *et al.*

Figure 2 of the geometric relationship shows that the angle ψ_r between the detonation wave front and the charge symmetry axis at the beginning of collision is

$$\alpha = \arctan \left(\frac{\tan \psi_0}{(\tan^2 \psi_0 + 1)\gamma + 1} \right), \quad (5)$$

where R_i is the distance between the initiation point and the charge symmetry axis and H_i is the distance between the projected point of the initiation point on the charge symmetry axis and the crossing point of the detonation wave front and the charge symmetry axis.

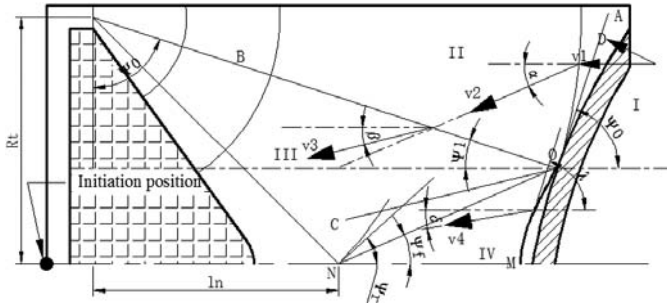


Figure 2. The detonation wave propagation and reflection when it formed at initiation top point of charge.

When the unreacted explosive in Area I (Fig. 2) located on the right side of the detonation wave front OA shoots askew with the incident angle ψ_0 toward the interface at high speed D , in point O the explosive flow parallel to the interface passing through the detonation wave front OA at speed V_1 . The explosive flow then deflects through an angle α (turning inward) and enters area II. From C-J detonation theory and the relevant geometric relationships¹³, it is deduced that

$$\alpha = \arctan \left(\frac{\tan \psi_0}{(\tan^2 \psi_0 + 1)\gamma + 1} \right) \quad (6)$$

$$M_2 = \sqrt{1 + \frac{\gamma + 1}{\gamma} \cdot \cot^2 \psi_0} \quad (7)$$

where γ is the exponent of the product of explosive gas, and M_2 is the Mach number of area II.

As the product of explosive gas continues moving to the reflected shock front OB , it turns outward in a counterclockwise direction through an angle $(\alpha - \beta)$ and flows into area III at speed V_3 . According to the mass conservation and momentum conservation of the product of the gas that flows in and out of the two sides of the reflected shock front OB , the Rankine-Hugoniot formula of the shock wave and the relevant geometric relationships, when the shock wave collides askew into area III, the pressure P_3 has the relationship

$$\frac{P_3}{P_H} = \frac{2\gamma}{\gamma + 1} M_2^2 \sin^2(\psi_1 + \alpha) - \frac{\gamma - 1}{\gamma + 1}, \quad (8)$$

where P_H is the pressure of the C-J detonation wave front and ψ_1 is the intersection angle of reflected shock waves.

When the incident angle ψ_0 of the shock front increases

to a certain angle, the denotation product passes through the reflected shock front OB at speed V_2 . The turning angle $(\alpha - \beta)$ now surpasses the maximum turning angle that the denotation product can make. Therefore, the material piles up, and the reflected shock waves are pushed away from the wall at a certain distance, resulting in irregular Mach reflection. At this time, area III can be divided into new areas III and IV by the slip line OC . In Fig. 2, the Mach stem is denoted OM , the speed is V_4 , the turning angle is δ , and the angle between the Mach stem and the incoming flow is λ ($\psi_0 < \lambda < 0.5\pi$). It follows that

$$\frac{P_4}{P_H} = \frac{\sin^2 \lambda}{\sin^2 \psi_0} \left(1 + \sqrt{1 - \frac{\eta \sin^2 \psi_0}{\sin^2 \lambda}} \right), \quad (9)$$

where η is the coefficient of over compression, ranging from 1.1 to 1.2.

This study refers to Dunne's work¹⁴ by selecting 45.61° as the starting point of the Mach reflection of denotation waves. Figure 3 is a graph of the pressure of denotation waves that produce regular and irregular reflections versus the incidence angle drawn according to Eqns (8) and (9).

Figure 3 shows that the wave shaper generates denotation waves that have regular or irregular collisions during transmission and greatly increased pressure, which results in the collapse of the liner under the large denotation load and the formation of the JPC.

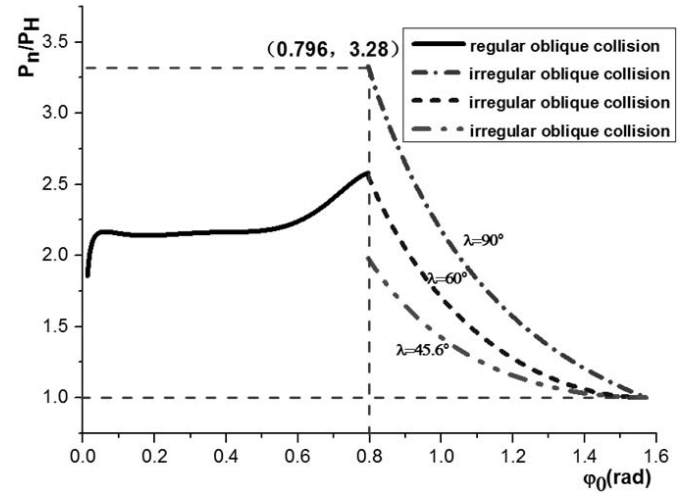


Figure 3. Pressure of denotation waves versus incidence angle.

3. EFFECT OF THE LINER CONFIGURATION PARAMETERS

To study the effect of the configuration parameters of the liner on the formation of dual-mode penetrators using the above methods, a simulation calculation model is built for a specific charge structure, and the effects of the liner configuration parameters on the formation of dual-mode penetrators are studied employing LS-DYNA finite element simulation software.

3.1 Simulation Model and Calculation Plans

Figure 4 shows a simulation model of a subcaliber charge structure and a wave shaper, where the charge diameter D_k is 110 mm, the maximum outer radius D_1 of the mouth of the

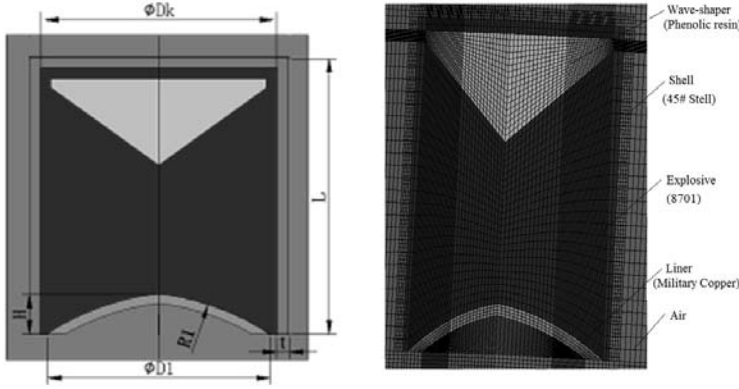


Figure 4. Simulation model of a subcaliber charge structure and wave shaper.

liner is $0.91 D_k$, the thickness t of the charge shell is $0.046 D_k$, and other parameters are taken from Chuang¹⁵, *et al.* on K charge jets. The liner is designed as an eccentric hemisphere with uniform thickness. The curvature radius of the outer arc of the liner is denoted R_1 . The thickness of the liner is denoted h and the height of the top of the liner H . In the simulation, the ALE algorithm is applied to calculate the penetrator formation with consideration of large changes of the grid and material flow. Calculations for the explosive, wave shaper, liner, and air are made using the Euler algorithm, while a fluid–solid coupling algorithm is used to calculate the mutual effects of the explosive, wave shaper, liner, air and shell. Finally, in the simulation of the JPC formation in the model, the key words CONTROL_EXPLOSIVE_SHADOW¹⁶ are added to control flame proofness and detonation diffraction.

Assuming that parameters of the charge structure and wave shaper have been determined, this study first determines the approximate scope of liner parameters according to the above theory and relevant literature. Simulations are then conducted for a curvature radius R_1 of the outer arc of the liner set from $0.85 D_k$ to $1.2 D_k$ (in intervals of $0.05 D_k$), a thickness h of the liner set from $0.030 D_k$ to $0.044 D_k$ (in intervals of $0.002 D_k$), and a height H of the top of the liner set from $0.146 D_k$ to $0.209 D_k$ (in intervals of $0.009 D_k$). The effect of each structural parameter on the formation of the EFP and JPC is investigated.

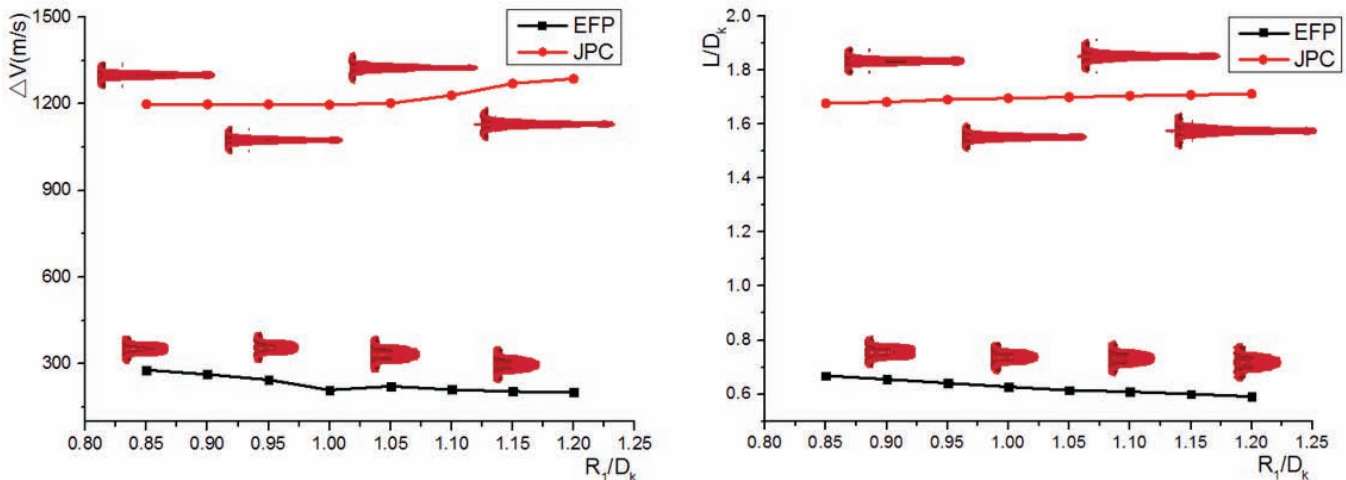


Figure 5. Forms of dual-mode penetrators and curves showing the effect of the curvature radius on formation parameters.

3.2 Curvature Radius of the Liner Outer Arc

To investigate the effects of the curvature radius R_1 of the outer arc of the liner on the formation of dual-mode penetrators, thickness h of the liner is set as $0.04 D_k$ and height H of the top of the liner as $0.173 D_k$. In simulation, the form of dual-mode penetrators and the relationships between parameters of penetrator formation and the curvature radius, as shown in Fig. 5.

As the curvature radius of the outer arc of the EFP increases, the cavity portion of the solid head gradually decreases, and the mass ratio of the solid head increases. However, the length of the solid head gradually reduces, which decreases the penetration depth of the EFP but increases the diameter of the EFP and the residual effect. As the curvature radius of the outer arc of the EFP increases, the cavity portion of the inner part of the EFP gradually decreases and vanishes, the shape of the JPC tends to stabilise, the velocity difference between the front and end decreases and the increasing level of the length–diameter ratio decreases. Therefore, considering the formed shape, the velocity difference between the front and end, and the length–diameter ratio of the penetrators, the paper chooses a curvature radius of the outer arc of the liner between $1.00 D_k$ and $1.15 D_k$.

3.3 Liner Shell Thickness

To analyse the effect of the liner shell thickness, the study takes the liner outer arc D_k as R_1 and the liner shell height as $0.173 D_k$. In simulation, Fig. 6 presents the form of dual-mode penetrators and the relationships between penetrator parameters and the liner shell thickness,

As the liner shell increases, the velocity difference between the head and tail of the dual-mode penetrator and the length/diameter ratio steadily decline, the EFP penetrator length decreases, the tail warped part grows, the inner cavity part shrinks and the mass of the head solid part increases, enhancing flight stability. The cavity part of the JPC penetrator gradually shrinks, reducing the penetrator effective mass. Therefore, considering the penetrator formation, the velocity difference between head and tail and the length–diameter ratio, the study chooses a liner shell thickness between $0.034 D_k$ and $0.040 D_k$.

3.4 Liner Top Height

According to foregoing modelling results, the study chooses the liner outer arc radius as R_l/D_k and the liner shell thickness h as $0.04 D_k$ to study the effect of the liner top height on the dual-mode penetrator formation. In simulation, the relationship between the dual-mode penetrator formation parameters and liner top height was shown in Fig. 7.

As the liner top height increases, the velocity difference between the head and tail of the dual-mode penetrator and the length/diameter ratio gradually increase, the cavity part of the penetrator formation shrinks, and the mass of the head solid part increases. When the liner height reaches $0.173 D_k$, the increase rate suddenly increases with head and tail velocity difference enlarged, leading to stretching of the penetrator, which can fracture during flight. Considering the penetrator formation, the velocity difference between the head and tail and length/diameter ratio, the paper chooses a liner top height between $0.164 D_k$ and $0.182 D_k$.

4. FORMATION OPTIMISATION AND DETONATION PRESSURE CALCULATION

On the basis of the foregoing theory and simulation, we obtain the ranges of reference parameters for single-detonation penetrator transformation from the EFP to JPC. However, for a specific initiation structure, parameters are still needed to optimise for obtaining a set of optimised parameters and thus a dual-mode penetrator with better shape. In the following, an optimised set of parameters through orthogonal optimisation of simulation results were obtained. Additionally, the study

analyse the detonation pressure during the process of penetrator formation, both theoretically and numerically.

4.1 Optimisation of Penetrator Formation

An orthogonal optimisation table with value ranges of parameters of a partial-hemisphere-shaped charge uniform wall thickness was constructed. The parameters are the outer radius R_l , liner height H , and liner wall thickness h . Table 1 lists the parameters and their corresponding value ranges. Each set of parameters is used in a numerical simulation employing LS-DYNA.

Table 1. Orthogonal optimisation parameters and their values

Group	R_l/D_k	H/D_k	h/D_k
1	0.955	0.136	0.03
2	1.0	0.155	0.033
3	1.046	0.173	0.036
4	1.091	0.191	0.038
5	1.136	0.209	0.041

The penetrator head velocity V_j and head-tail velocity difference ΔV for both the EFP and JPC were obtained by simulation. then the order of the effects of different parameters on different targets in extreme difference analysis was obtained, as shown in Table 2.

The order of effects on the targets given in Table 2 clearly shows that the liner wall h is the most important parameter affecting the head velocity difference V_j for the EFP and JPC,

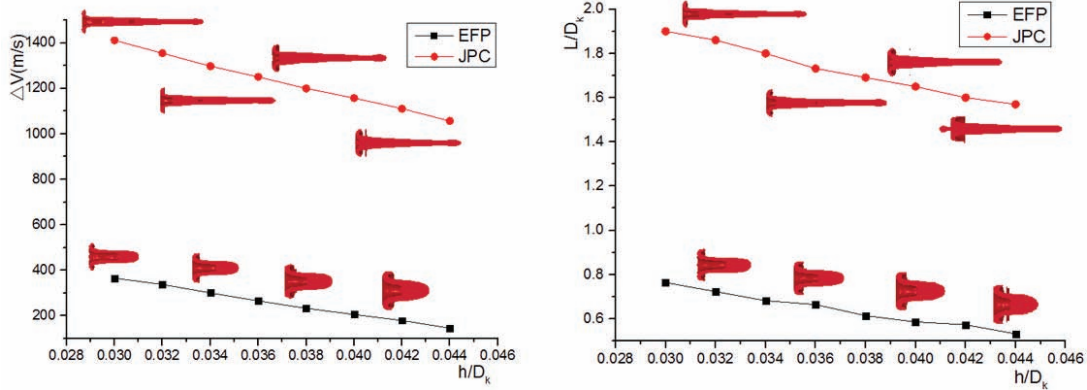


Figure 6. Forms of dual-mode penetrators and curves showing the effect of the liner shell thickness on formation parameters.

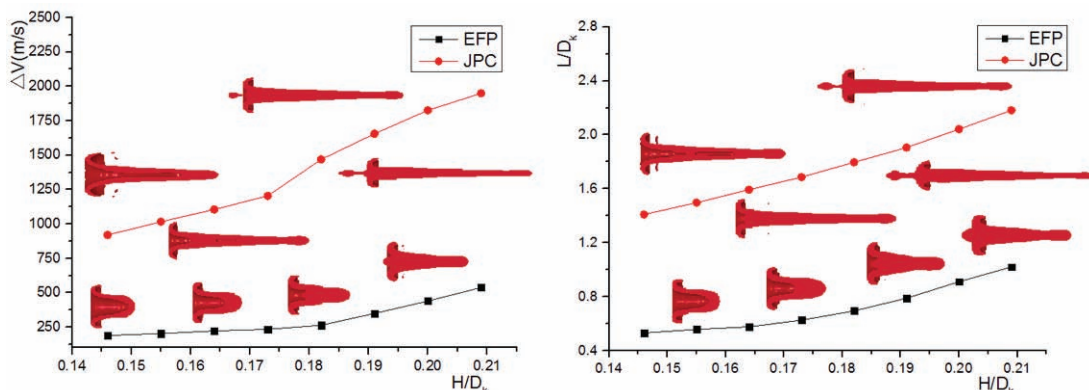


Figure 7. Forms of dual-mode penetrators and curves showing the effect of the liner top height on formation parameters.

Table 2. Order of effects on different targets

Item	Effects of V_j	Effects of ΔV
EFP	$h > H > R_1$	$H > h > R_1$
JPC	$h > R_1 > H$	$R_1 > h > H$

but different affects the head–tail velocity difference ΔV for the EFP and JPC. Thus it is necessary for us to analyse the influence of index in every dependent factor and obtain suitable structural parameters of liner. As shown in Fig. 8, the change curve of formation parameters of penetrators with factors was presented. A, B and C respectively stand for the parameters of outer radius R_1 , liner height H , and liner wall thickness h and 1, 2, 3, 4 and 5, respectively stand for five indexes in every dependent factor. So we can study the influence law of two indexes in every dependent factor, and know the difference of same index in different dependent factor.

Through analysis the Table 2 and Fig. 8, the result which the liner outer radius R_1 is the most important parameter affecting the head–tail velocity difference ΔV for the JPC can be obtained. A larger R_1 corresponds to a higher head velocity V_j and greater head–tail velocity difference ΔV . When guaranteeing a high head velocity, it needs to control the head–tail velocity difference ΔV . Thus R_1 was set as $1.09 D_k$.

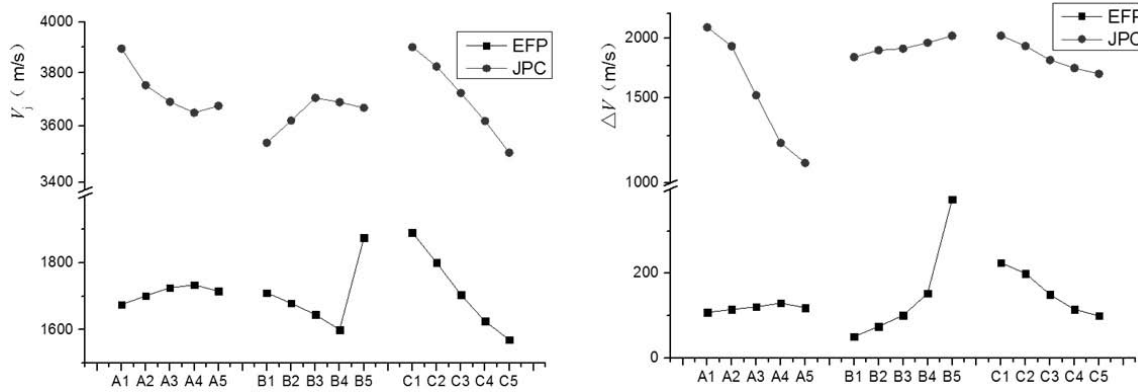
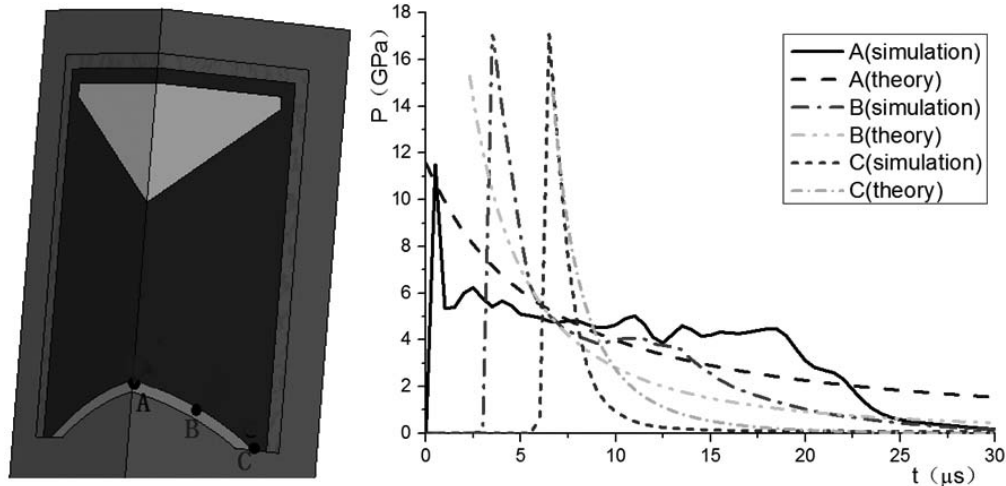
The liner height H is the most important parameter affecting the penetrator head–tail velocity difference. As H increases, the EFP penetrator head–tail velocity difference ΔV

increases. To ensure flight stability, a relatively small head–tail velocity is desired. As for the JPC penetrator, the effect of the liner height is quite weak. Therefore, the liner height H is set as $0.173 D_k$.

Finally, for both EFP and JPC penetrators, the thickness of the liner wall h is the most important parameter affecting the head velocity V_j and the second most important parameter affecting the head–tail velocity difference ΔV . As h decreases, the penetrator head velocity V_j and head–tail velocity difference ΔV increase. To ensure the stretch and thus flight stability of the penetrator, h cannot be too small or too large. Generally, h is taken as $0.036 D_k$.

4.2 Calculation of the Detonation Pressure

In this section, the pressure variation conditions at the same liner surface by comparing analytical and numerical simulation results were analysed. For the case of initiation at the top of shaped charge liner, the detonation pressure at points A, B, and C was computed, as shown in Fig. 9. There is a considerable difference between analytical and numerically calculated maximum pressure values mainly owing to the shaped charge shell. The mechanism of liner top initiation forming the EFP penetrator is valid, because the difference is within 5 per cent and the pressure curves have the same trend. Additionally, both the analytical and numerical simulation results give pressure curves indicating that detonation pressure on the liner surface is comparatively low, but more even, which


Figure 8. The change curve of formation parameters of penetrators with factors.

Figure 9. Pressure at different points according to analytical and numerical analyses with liner top initiation.

benefits the formation of a stable EFP.

For initiation at the center of charge, detonation pressure at points D, E, F, G, and H, was computed as shown in Fig. 10. Comparing pressure curves in Fig. 10 and Fig. 3, it can find that the difference between analytical and numerical maximum detonation pressures is only 3 per cent. According to the analytical calculation, the incidence angle increases from point D to point E, but detonation pressure decreases and approaches the C-J detonation pressure P_H , which coincides with the maximum numerical value. Additionally, comparing Figs. 9 and 10, it presents higher detonation pressure can be derived with the liner top center initiation.

Finally, simulations for dual-mode penetrator formation, the penetrator head velocity V_j were conducted, and the penetrator length L using the obtained analytical and numerical optimised liner structure; results are given in Table 3.

Table 3. Dual-mode penetrator formation and numerical results (200 μ s)

Damage element	Forming diagram	V_j (m/s)	L (mm)
EFP		1692	72
JPC		3725	292.5

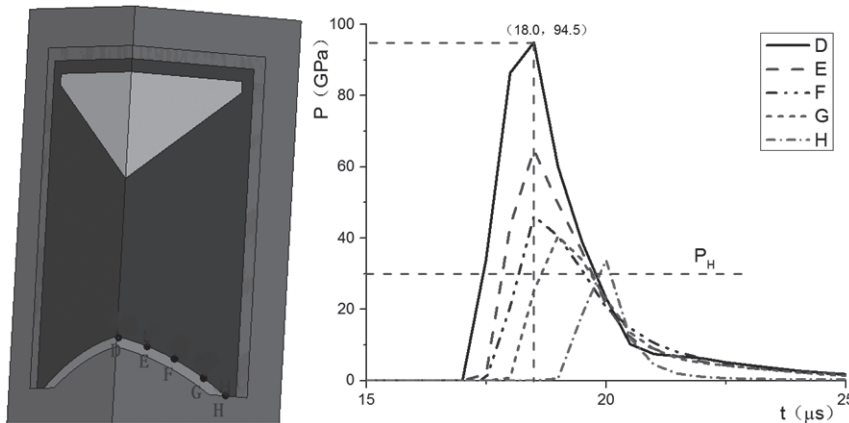


Figure 10. Pressure at different points according to analytical and numerical analyses with liner top initiation.

5. EXPERIMENTAL VALIDATION

To validate the dual-mode penetrator transformation from the EFP to the JPC by changing the detonation location of the optimised uniform-wall-thickness flat eccentric hemisphere liner with wave shaper, the same parameters were used as used in the simulation to conduct an experiment with X-ray imaging. Different penetrator formations at different times were obtained from the X-ray analysis. The top detonation generated an EFP, while the liner top center detonation generated a JPC. With all parameters varying by no more than 10 per cent, X-ray imaging is compared with simulation results in Table 4, where V_j is the velocity of the penetrator head, V_s is the tail velocity, l_1 is the penetrator length, and d_1 is the penetrator diameter. To realise the formation of the EFP penetrator with liner top detonation, a through-hole at the liner top that has the same diameter as the detonator were opened. In this way, the detonator can initiate the main charge. As a result of the through-hole and detonator, X-ray imaging shows fracture of the penetrator head.

The experiment also evaluated the penetration power of dual-mode penetrators. The study selected a burst height of 13 D_k . Results are presented in Fig. 11. For liner top detonation, the EFP penetrator had a penetration depth of 0.64 D_k and a maximum penetration diameter of 0.62 D_k . Meanwhile, the liner top center detonation generated a JPC that perforated the first target with a maximum diameter of 0.32 D_k and formed a penetration tunnel that was comparatively even, and had a penetration depth of 0.6 D_k and maximum penetration diameter of 0.27 D_k for the second target, giving a total penetration depth of 2.42 D_k . Therefore, the liner structure used in this study can generate an EFP and JPC having good penetration power as dual-mode penetrators.

6. CONCLUSIONS

- (i) The present study designed a new type of dual-mode penetrator warhead structure. By changing the detonation position of the liner, a suitable EFP and JPC can be generated.
- (ii) A theoretical model was constructed to analyse the EFP and JPC detonation pressures and to determine the liner surface pressures under different detonation conditions.

Table 4. Experimental and numerical comparison of the dual-mode penetrator formation

Item	Method	Forming diagram	V_j (m/s)	V_s (m/s)	l_1 (mm)	d_1 (mm)
EFP (120 μ s)	simulation		1783	1538	70.5	54.8
	test		1875	1625	65	60
JPC (80 μ s)	simulation		3854	2379	128.5	68
	test		4000	2500	123.14	73.36

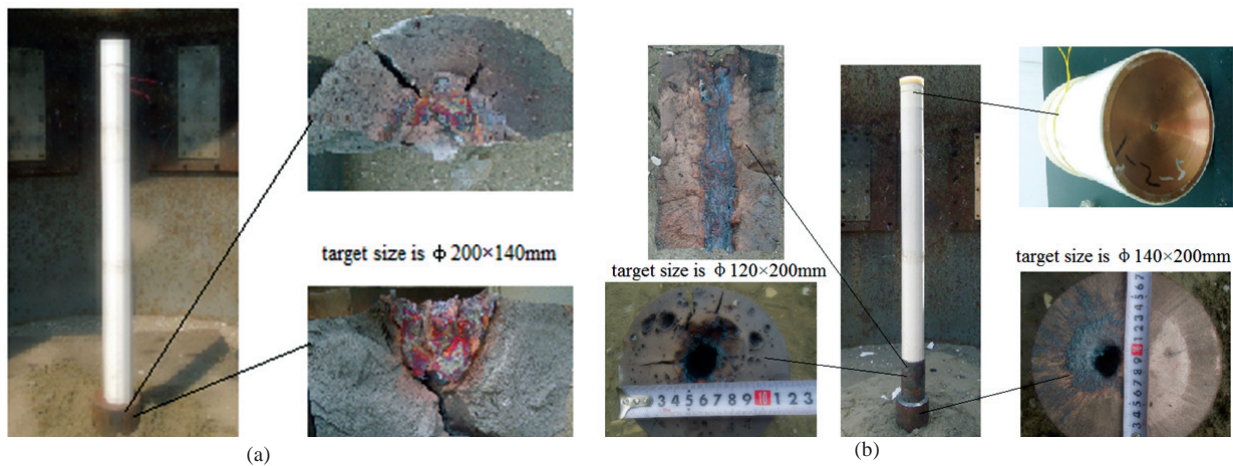


Figure 11. Experiments on the penetration of a steel target by dual-mode penetrators with burst height of $13 D_k$ (a) Penetration effect of the EFP and (b) Penetration effect of the JPC

- (iii) The effects of liner structural parameters on the dual-mode penetrators were investigated. The parameter ranges of an optimised uniform-wall-thickness flat eccentric hemisphere liner with a wave shaper were found to be an outer radius R_1 of $1.00 D_k - 1.15 D_k$, wall thickness h of $0.034 D_k - 0.040 D_k$, and liner height H of $0.164 D_k - 0.182 D_k$.
- (iv) A set of liner structural parameters were obtained by orthogonal optimisation design. The results of X-ray imaging and penetration power experiments validated the simulation results. With a burst height of $13 D_k$, the EFP can penetrate a steel target to a depth of $0.64 D_k$ and the JPC, a steel target to a depth of $2.42 D_k$.

REFERENCES

- Richard, Fong. New, selectable, explosively formed penetrator (EFP) warhead concept. *In* 41st Annual Bomb & Warhead Technical Meeting, 1991. Naval Ocean Systems Center, San Diego CA, pp.172-197.
- Robert, J. Lawther Dual operating mode warhead US Patent: 5509357, 1996.
- Bender, D.; Fong, R. & Ng, W. Dual mode warhead technology for future smart munitions. *In* Proceedings of the 19th international symposium on ballistics: Interlaken, Switzerland, 2001, pp. 679-684.
- Whelan, A.J.; tephau, B. & James, W. Multiple effect warheads for defeat of urban structures and armour. *In* Proceedings of the 24th international symposium on ballistics: New-Orleans, Louisiana, 2008, 1092-1098.
- Li, W.B.; Wang, X.M. & Li, W.B. The effect of annular multi-point initiation on the formation and penetration of an explosively formed penetrator. *Int. J. Impact Eng.*, 2010, **37**(4), 414-424. doi: 10.1016/j.ijimpeng.2009.08.008
- Graswald, M. & Arnold, W. Experimental studies of scalable effects warhead technologies. *In* Proceeding 26th International Symposium on Ballistics: Miami, Florida, USA, 2011, pp 286-296.
- Arnold, W. & Graswald, M. A novel technology for switchable modes warheads. *In* Proceeding 26th International Symposium on Ballistics: Miami, Florida, USA, 2011.
- Weibing, Li.; Xiaoming, Wang.; Wenbin, Li. & Y, Zheng. Research on the optimum length-diameter ratio of the charge of a multimode warhead. *Shock Waves*, 2012, **22**, 265-274. doi: 10.1007/s00193-012-0365-z
- Beijing Institute of Technology: Explosion and action. Defence Industry Press, Beijing, 1979.
- Cao, Bing. The research on the EFP formation mechanism and related key techniques. Nanjing University of Science and Technology Nanjing 2001. doi: 10.7666/d.y469019
- Zhang, Baoping. Detonation Physics: Weapon Industry Press, Beijing, 2009.
- Yanguo, Zhang.; XianFeng, Zhang.; Yong, He. & Liang, Qiao. Detonation wave propagation in shaped charges with large wave-shape. *In* Proceeding 27th International Symposium on Ballistics: Germany, 2013.
- Xinli, Sun. Detonation shock dynamics: Northwestern Polytechnical University Press. Beijing, 2011.
- Dunne, B.B. Mach reflection of detonation waves in condensed high explosive. *Phys. Fluids*, 1961, **4**, 918. doi:10.1063/1.1706425
- Chuang, Chen.; WeiBing, Li.; Xiaoming, Wang. & Wenbin, Li. The optimization design of precursor K charge structure of tandem warhead. *Chinese J. High Pressure Phy.*, 2014, **28**(1), 73-78 (Chinese). doi:10.11858/gywlx.2014.01.012
- Livermore. LS-DYNA Keyword User's Manual. California: Livermore Software Technology Corporation, USA, 2007.

ACKNOWLEDGMENTS

This research was sponsored by the Nature Science Foundation (Project No. 11202103) and sponsored by Qing Lan Project.

CONTRIBUTORS

Prof. Wei-bing Li received his PhD (Mechanical Engineering) from Nanjing University of Science & Technology, in 2011. Currently, he is Associate Professor affiliated to the School of Mechanical Engineering, Nanjing University of Science & Technology, Nanjing. His research areas include: Explosion mechanics,

terminal ballistics, vulnerability and survivability.

His contribution in the current study, he design of whole thought and experiment research.

Mr Huan Zhou received his Master (Mechanical Engineering) from Nanjing University of Science & Technology, in 2014. He was involved in the Transformation of dual-mode EFP and JPC in the shaped charge with wave shaper and its typical damage of tank target.

His contribution in the current study in algorithm of numerical simulation.

Prof. Wen-bin Li received his PhD (Mechanical Engineering) from Nanjing University of Science & Technology, China. Currently, he is the Professor of the School of Mechanical Engineering. His research areas include: Explosion mechanics, terminal ballistics, vulnerability and survivability, ordnance science and technology.

His contribution in the current study in design of structure.

Prof. Xiao-Ming Wang received his PhD (Mechanical Engineering) from Nanjing University of Science & Technology, China. Currently, he is the Professor of the School of Mechanical Engineering, Nanjing University of Science & Technology, China. His research areas include: Explosion mechanics, terminal ballistics, vulnerability and survivability, ordnance science and technology.

His contribution in the current study in damage power of projectile.

Mr Jian-jun Zhu received Bachelor of Engineering (Ordnance Science and Technology) from Nanjing University of Science & Technology, in 2014. Currently pursuing his PhD from Nanjing University of Science & Technology, China.

His contribution in the current study in. the fracture of materials and structures under high strain rate.